ACS APPLIED MATERIALS & INTERFACES

www.acsami.org

Research Article

Controlled Synthesis of Poly[(3-alkylthio)thiophene]s and Their Application to Organic Field-Effect Transistors

Po-Shen Lin,[⊥] Yamato Shoji,[⊥] Shakil N. Afraj,[⊥] Mitsuru Ueda, Ching-Hsuan Lin, Shin Inagaki, Taiki Endo, Shih-Huang Tung, Ming-Chou Chen,* Cheng-Liang Liu,* and Tomoya Higashihara*

Cite This: *ACS Appl. Mater. Interfaces* 2021, 13, 31898–31909

Read Online

ACCESS | Metrics & More | Article Recommendations | Supporting Information

ABSTRACT: Regioregular polythiophenes have been widely used in organic electronic applications due to their solution processability with chemical modification through side chain engineering, as well as their microstructural organization and good hole transport properties. Here, we introduce alkylthio side chains, (poly[(3-alkylthio)thiophene]s; **P3ATTs**), with strong noncovalent sulfur molecular interactions, to main chain thienyl backbones. These **P3ATTs** were compared with alkyl-substituted polythiophene (poly(3-alkylthiophene); **P3AT**) variants such that the effects of straight (hexyl and decyl) and branched (2-ethylhexyl) side chains (with and without S atoms) on their thin-film morphologies and crystalline states could be investigated. **P3ATTs** with linear alkylthio side chains (**P3HTT**, hexylthio; **P3DTT**, decylthio) did not attain the expected higher organic field-effect transistor (OFET) mobilities with respect to **P3HT** (hexyl) and **P3DT** (decyl) mainly due to their lower regioregularity (76−78%), although **P3ATTs** exhibit an enhanced tendency for aggregation and compact molecular packing, as indicated by the red-shifting of the absorption spectra and the shortening of the $\pi-\pi$ stacking distance, respectively. Moreover, the loss of regioregularity issue can be solved by introducing more soluble 2-ethylhexylthio branched side chains to form poly[3-(2-ethylhexylthio)thiophene] (**P3EHTT**), which provides enhanced crystallinity and efficient charge mobility (increased by up to a factor of 3) with respect to the poly(2-ethylhexylthiophene) (**P3EHT**) without S atoms in the side moieties. This study demonstrates that the presence of side chain alkylthio structural motifs with nonbonded interactions in polythiophene semiconductors has a beneficial impact on the molecular conformation, morphologies, structural packing, and charge transport in OFET devices.

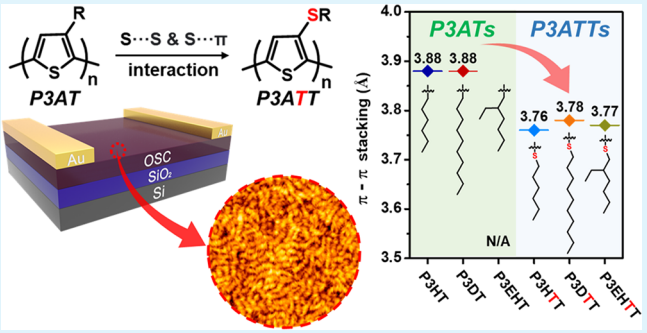

KEYWORDS: *polythiophene, organic field-effect transistor, noncovalent interaction, alkylthio side chain, molecular aggregation*

INTRODUCTION

Semiconducting polymers have received much attention due to their good solubility and excellent optoelectronic properties, enabling the development of low-cost, lightweight, flexible, and large-area electronic devices such as organic field-effect transistors (OFETs),[1−4] polymer solar cells (PSCs),[5−7] and thermoelectric films.[8−10] To achieve the functionalization of organic materials for such applications, special molecular designs for modulating the effective π-conjugation of semiconducting polymers have been developed.[11−15] For instance, recent studies have proposed the addition of a 3-alkylthio side chain in π-conjugated small molecules and polymers, where the introduction of a sulfur atom interposed between the thiophene heterocyclic rings and alkyl side chain substituents can help with controlling the molecular conformation.[16−27] Computational and experimental studies have shown that the thioether sulfur atom provides a directional nonbonded interaction with π-conjugated moieties (S···π) and neighboring sulfur atoms (S···S) on the same chain or neighboring chain.[28−33] Therefore, it is anticipated that the alkylthio side chain can facilitate the formation of a strong intra- and intermolecular noncovalent interaction in the π-conjugated system while maintaining the planarity of the π-molecules, promoting π-electron delocalization, and inducing diverse molecular aggregation, thus potentially enhancing the electrical properties.

The use of well-defined semiconducting polymers is important, as parameters such as the number-average molecular weight (M_n), molar-mass dispersity ($Đ_M$), and regioregularity (R.R.) have a significant effect on their performance and must be optimized before determining the optoelectronic characteristics. Regioregular poly(3-alkylthiophene)s (**P3ATs**)[34−38] are well-characterized bench-

Received: March 8, 2021
Accepted: June 1, 2021
Published: June 30, 2021

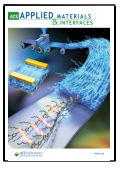

https://doi.org/10.1021/acsami.1c04404
ACS Appl. Mater. Interfaces 2021, 13, 31898−31909

mark *p*-type semiconducting polymers due to their excellent balance of crystallinity and solubility. The discovery of the chain-growth mechanism in the Ni-catalyst-transfer polycondensation (also called Grignard metathesis (GRIM) polymerization) system has made it possible to supply well-defined **P3AT** with predicted M_n, low $Đ_M$, and high R.R. up to 99%.[39−42] Regardless of the tremendous effort expended on such controlled polymerization, **P3AT** exhibits only moderate performance; for example, an OFET mobility of $\sim 10^{-1}$ cm V^{-1} s^{-1}[43] and a power conversion efficiency (PCE) of around 4−5% were obtained in bulk-heterojunction (BHJ)-type PSCs based on the **P3AT**:[6,6]-phenyl C_{61} butyric acid methyl ester (PCBM) blend system.[44]

The use of alkylthio side chain substituents in poly(thiophene)s, namely, poly[(3-alkylthio)thiophene] (**P3ATT**), is of great interest because of the dual potential applicability of strong S···S chalcogen−chalcogen and S···π intra/intermolecular interactions and controlled polymerization. Rieke and co-workers synthesized regioregular head-to-tail **P3ATT** (R.R. ∼90%) with moderate M_n values of ∼6k through the Ni-catalyzed polymerization of 3-alkylthio-2-bromo-5-(bromozincio)thiophenes via the regioselective oxidative addition of Rike zinc (Zn*) to 3-alkylthio-2,5-dibromothiophenes.[45] Koeckelberghs and co-workers improved the M_n value of **P3ATT** up to 9.6k (regioregular) and 17.5k (regio-irregular) by introducing the 3,7-dimethyloctyl branched side chain using the ″modified McCullough method″ and GRIM polymerization, respectively.[46] There seems to be a trade-off between M_n and R.R. of **P3ATT**, as higher R.R. generally corresponds to lower solubility, probably due to an increased number of coplanar π-conjugated structures. Thus, it prevents the propagation reaction by unwanted precipitation of **P3ATT** during polymerization, resulting in limited M_n. Swager et al. synthesized **P3ATT** with very high M_n (54.6k) with a high R.R. of 96% via dehydrobrominative polymerization employing 3-alkylthio-2-bromothiophene as a monomer and Knochel's base[47] for regioselective dehydration at the 5-position of the thiophene ring.[48] This success may arise from the design of the 2-butyloctyl group as a bulky side chain. These **P3ATT**s were utilized as precursors for poly[3-(alkylsulfone)thiophene], exhibiting a large Faraday effect with Verdet constants up to $(7.63 \pm 0.78) \times 10^4$ deg T^{-1} m^{-1}. Regardless of the considerable previous effort toward the controlled synthesis of **P3ATT**s, unfortunately, no information regarding the mobilities of **P3ATT** has been reported except for an octamer of head-to-head/tail-to-tail alkylthiothiophene exhibiting a hole mobility of $\sim 10^{-5}$ cm^2 V^{-1} s^{-1}.[49] Note that Li and co-workers reported PSCs fabricated with **P3ATT** as a donor and PCBM as an acceptor (1:1, w/w) showing a relatively low PCE of 0.34%;[50] however, there is a lack of reports regarding the OFET mobility of **P3ATT**. Overall, in these **P3ATT** molecular frameworks, the fine modulation of S···S and S···π interactions along the polythiophene backbone influences the interchain organization, film morphology, and electronic properties.

Herein, we describe the synthesis of well-defined **P3ATT** polymers via GRIM polymerization or dehydrohalogenative polymerization using Knochel's base[35] to elucidate their OFET characteristics in comparison with those of regioregular poly(3-alkylthiophene) (**P3AT**) prepared using dehydrohalogenative polymerization. To enhance the solubility of the **P3ATT**s, three different side chains (R = $-SC_6H_{13}$, $-SC_{10}H_{21}$, and $-SC_8H_{17}$(br)) were installed and assessed to determine the criteria for the trade-off between the R.R. and M_n values. Therefore, the modification of the side chains in polythiophenes was systematically studied, including the variation of the side chain from hexyl to longer or branched chains, as well as the replacement of the bridging carbon with a sulfur atom, to boost the interchain packing, thin-film morphology, and charge transport properties. To the best of our knowledge, the OFET characteristics of **P3ATT**s have not yet been clarified.

EXPERIMENTAL SECTION

Materials. All reagents and solvents were commercial products purchased from Sigma-Aldrich, TCI, and Wako Pure Chemical Industries, Ltd., and used without further purification. Tetrahydrofuran (THF, 99.5%, Kanto Chemical Co., Inc.) was refluxed over sodium benzophenone under nitrogen for 2 h and then distilled immediately before use.

Measurements. ^{1}H nuclear magnetic resonance (^{1}H NMR) spectra for polymer characterization and determination of R.R. were recorded on a JEOL JNM-ECX400 (400 MHz) in deuterated chloroform-d_1 ($CDCl_3$) at 25 °C, calibrated to chloroform as a standard (δ_H 7.24), or on a JEOL JNM-ECX600 (600 MHz) in deuterated 1,1,2,2-tetrachloroethane-d_2 ($C_2D_2Cl_4$) at 100 °C, calibrated to 1,1,2,2-tetrachloroethane as a standard (δ_H 6.00). The number average and weight average molecular weights (M_n and M_w) and molar-mass dispersity ($Đ_M$) were measured via size exclusion chromatography (SEC) using a JASCO GULLIVER HPLC system equipped with a pump (JASCO PU-1580), a column oven (JASCO CO-2065Plus), a UV detector (λ = 254 nm, JASCO UV-1575), and an RI detector (RI-1580). The column set was as follows: a guard column (Shodex KF-G) and two consecutive columns (Shodex KF-804L and Shodex KF-805L) eluted with THF at 40 °C at a flow rate of 1.0 mL min^{-1}. Polystyrene standards were used for the calibration. Thermal analysis was performed on an SII EXSTAR 6000 system, thermogravimetry (TG) was performed with a TG/DTA 6300 thermal analyzer at a heating rate of 10 °C min^{-1}, and differential scanning calorimetry (DSC) was performed using a DSC 6200 thermal analyzer connected to a cooling system at a heating/cooling rate of 10 °C min^{-1}. UV−vis absorption spectra were recorded on a JASCO V-670 UV−vis spectrophotometer. Polarized optical microscopy (POM) images were obtained using a Leica 2700 M microscope equipped with a Nikon digital camera. Photoelectron spectroscopy in air (PESA) measurements were recorded using a Riken Keiki AC-2 PESA spectrometer. Atomic force microscopy (AFM) measurements were carried out in the tapping mode on an SPA-400 under ambient conditions. Grazing incidence X-ray diffraction (GIXRD) measurements were performed at the National Synchrotron Radiation Research Center (NSRRC) of Taiwan on the beamline 13A1/17A1/23A1.

General Synthetic Procedure for Poly[3-(hexylthio)-thiophene] (P3HTT). In a 100 mL round-bottom flask purged with N_2, 2,5-dibromo-3-(hexylthio)thiophene (∼0.6 g, ∼1.7 mmol) was dissolved in dehydrated THF or dehydrated 1,4-dioxane (60 mL). To this solution was added a THF solution of a stoichiometric amount of isopropylmagnesium chloride·lithium chloride (^{i}PrMgCl·LiCl) (1.3 M, ∼1.3 mL, ∼1.7 mmol) at 0 °C. The Grignard exchange reaction was performed at a set temperature (room temperature, 40 °C, 60 °C, or 100 °C) for 30 min. To the reaction mixture, 1,3-bis(diphenylphosphino)propanenickel(II) dichloride (Ni(dppp)-$Cl_2$$M_n$) was added, which was prepared just before use by mixing bis(triphenylphosphine)nickel(II) dichloride ($Ni(PPh_3)_2Cl_2$) and 2 equiv of 1,3-bis(diphenylphosphino)propane (dppp) in dehydrated THF (4 mL) in a 20 mL round-bottom flask purged with N_2. The mixture was allowed to stand at the set temperature (room temperature, 40 °C, 60 °C, or 100 °C) for 3 h to undergo polymerization. After quenching the polymerization with 5 M aq HCl (1 mL), the solution was poured into methanol/water (300:100 mL) in a 500 mL beaker to precipitate the polymer. After filtration, the collected polymer was purified by Soxhlet extraction with methanol, acetone, and hexane and recovered with chloroform. The chloroform

https://doi.org/10.1021/acsami.1c04404
ACS Appl. Mater. Interfaces 2021, 13, 31898−31909

solution was passed through a short silica gel column to remove residual metal contaminants and condensed using a rotary evaporator followed by freeze-drying from its absolute benzene solution to afford the purified polymer (**P3HTT**) as a purple-colored powder.

P3HTT (8k). Grignard exchange reaction/polymerization: in THF at room temperature. Yield: 0.039 g, 12%. M_n (target) = 30,000, M_n (SEC) = 8300, $Đ_M$ = 1.33. R.R. = 84%. ^{1}H NMR (600 MHz, $C_2D_2Cl_4$, δ, ppm): 7.43 (s, Th-4*H* (H-T)), 7.30−7.05 (m, Th-4*H* (H-H/T-T)), 2.97 (m, $-SCH_2-$), 1.73 (m, $-SCH_2CH_2-$), 1.48 (m, $-SCH_2CH_2CH_2-$), 1.32 (m, $-CH_2CH_2CH_3/-CH_2CH_3$), 0.92 (m, $-CH_3$).

P3HTT (10k). Grignard reaction/polymerization: in THF at 60 °C. Yield: 0.114 g, 36%. M_n (target) = 10,000, M_n (SEC) = 10,400, $Đ_M$ = 1.40. R.R. = 74%. ^{1}H NMR (600 MHz, $C_2D_2Cl_4$, δ, ppm): 7.43 (s, Th-4*H* (H-T)), 7.30−7.05 (m, Th-4*H* (H-H/T-T)), 2.97 (m, $-SCH_2-$), 1.75−1.68 (m, $-SCH_2CH_2-$), 1.48 (m, $-SCH_2CH_2CH_2-$), 1.34 (m, $-CH_2CH_2CH_3/-CH_2CH_3$), 0.92 (m, $-CH_3$).

P3HTT (13k). Grignard reaction/polymerization: in THF at 40 °C. Yield: 0.081 g, 25%. M_n (target) = 30,000, M_n (SEC) = 13,200, $Đ_M$ = 1.47. R.R. = 78%. ^{1}H NMR (600 MHz, $C_2D_2Cl_4$, δ, ppm): 7.43 (s, Th-4*H* (H-T)), 7.30−7.05 (m, Th-4*H* (H-H/T-T)), 2.98 (m, $-SCH_2-$), 1.73 (m, $-SCH_2CH_2-$), 1.47 (m, $-SCH_2CH_2CH_2-$), 1.34 (m, $-CH_2CH_2CH_3/-CH_2CH_3$), 0.92 (m, $-CH_3$).

P3HTT (14k). Grignard reaction/polymerization: in THF at 60 °C. Yield: 0.207 g, 66%. M_n (target) = 15,000, M_n (SEC) = 14,000, $Đ_M$ = 1.47. R.R. = 77%. ^{1}H NMR (600 MHz, $C_2D_2Cl_4$, δ, ppm): 7.43 (s, Th-4*H* (H-T)), 7.30−7.05 (m, Th-4*H* (H-H/T-T)), 2.98 (m, $-SCH_2-$), 1.73 (m, $-SCH_2CH_2-$), 1.47 (m, $-SCH_2CH_2CH_2-$), 1.34 (m, $-CH_2CH_2CH_3/-CH_2CH_3$), 0.92 (m, $-CH_3$).

P3HTT (15k). Grignard reaction/polymerization: in THF at 60 °C. Yield: 0.098 g, 29%. M_n (target) = 50,000, M_n (SEC) = 15,000, $Đ_M$ = 1.50. R.R. = 76%. ^{1}H NMR (600 MHz, $C_2D_2Cl_4$, δ, ppm): 7.43 (s, Th-4*H* (H-T)), 7.30−7.05 (m, Th-4*H* (H-H/T-T)), 2.98 (m, $-SCH_2-$), 1.73 (m, $-SCH_2CH_2-$), 1.47 (m, $-SCH_2CH_2CH_2-$), 1.34 (m, $-CH_2CH_2CH_3/-CH_2CH_3$), 0.92 (m, $-CH_3$).

P3HTT (20k). Grignard reaction/polymerization: in 1,4-dioxane at 100 °C. Yield: 0.177 g, 54%. M_n (target) = 50,000, M_n (SEC) = 20,200, $Đ_M$ = 1.73. R.R. = 68%. ^{1}H NMR (600 MHz, $C_2D_2Cl_4$, δ, ppm): 7.43 (s, Th-4*H* (H-T)), 7.30−7.10 (m, Th-4*H* (H-H/T-T)), 2.97 (m, $-SCH_2-$), 1.75−1.68 (m, $-SCH_2CH_2-$), 1.47 (m, $-SCH_2CH_2CH_2-$), 1.34 (m, $-CH_2CH_2CH_3/-CH_2CH_3$), 0.92 (m, $-CH_3$).

General Synthetic Procedure for Poly[3-(decylthio)-thiophene] (P3DTT). In a 100 mL round-bottom flask purged with N_2, 2,5-dibromo-3-(decylthio)thiophene (∼0.4 g, ∼1.0 mmol) was dissolved in dehydrated THF (50 mL). To this solution was added a stoichiometric amount of THF solution of ^{i}PrMgCl·LiCl (1.3 M, ∼0.77 mL, ∼1.0 mmol) at 0 °C. The Grignard exchange reaction was performed at 60 °C for 30 min. To the reaction mixture was added a Ni(dppp)Cl_2 (depending on the target M_n) solution, which was prepared just before use by mixing $Ni(PPh_3)_2Cl_2$ and 2 equiv dppp to dehydrated THF (4 mL) in a 20 mL round-bottom flask purged with N_2. The mixture was allowed to stand at 60 °C for 3 h for polymerization. After quenching the polymerization with 5 M aq HCl (1 mL), the solution was poured into methanol/water (300:100 mL) in a 500 mL beaker to precipitate the polymer. After filtration, the collected polymer was purified by Soxhlet extraction with methanol, acetone, and hexane and recovered with chloroform. The chloroform solution was passed through a short silica gel column to remove residual metal contaminants and condensed using a rotary evaporator followed by freeze-drying from its absolute benzene solution to afford the purified polymer (**P3DTT**) as a purple-colored powder.

P3DTT (10k). Yield: 0.038 g, 26%. M_n (target) = 20,000, M_n (SEC) = 10,100, $Đ_M$ = 1.25. R.R. = 86%. ^{1}H NMR (600 MHz, $C_2D_2Cl_4$, δ, ppm): 7.43 (s, Th-4*H* (H-T)), 7.30−7.10 (m, Th-4*H* (H-H/T-T)), 2.97 (m, $-SCH_2-$), 1.73 (m, $-SCH_2CH_2-$), 1.47 (m, $-SCH_2CH_2CH_2-$), 1.35−1.10 (m, other $-CH_2-$), 0.89 (m, $-CH_3$).

P3DTT (12k). Yield: 0.179 g, 63%. M_n (target) = 15,000, M_n (SEC) = 12,400, $Đ_M$ = 1.25. R.R. = 77%. ^{1}H NMR (600 MHz, $C_2D_2Cl_4$, δ, ppm): 7.43 (s, Th-4*H* (H-T)), 7.30−7.10 (m, Th-4*H* (H-H/T-T)), 2.96 (m, $-SCH_2-$), 1.72 (m, $-SCH_2CH_2-$), 1.45 (m, $-SCH_2CH_2CH_2-$), 1.35−1.10 (m, other $-CH_2-$), 0.89 (m, $-CH_3$).

P3DTT (18k). Yield: 0.187 g, 68%. M_n (target) = 20,000, M_n (SEC) = 17,700, $Đ_M$ = 1.29. R.R. = 78%. ^{1}H NMR (600 MHz, $C_2D_2Cl_4$, δ, ppm): 7.43 (s, Th-4*H* (H-T)), 7.30−7.10 (m, Th-4*H* (H-H/T-T)), 2.97 (m, $-SCH_2-$), 1.73 (m, $-SCH_2CH_2-$), 1.45 (m, $-SCH_2CH_2CH_2-$), 1.35−1.10 (m, other $-CH_2-$), 0.90 (m, $-CH_3$).

General Synthetic Procedure for Poly[3-(2-ethylhexylthio)-thiophene] (P3EHTT), Poly(3-hexylthiophene) (P3HT), Poly(3-decylthiophene) (P3DT), and Poly(2-ethylhexylthiophene) (P3EHT). In a 100 mL round-bottom flask purged with N_2, 3-(alkylthio/alkyl)-2-bromothiophene was dissolved in dehydrated THF (50 mL). To this solution was added a THF/toluene solution of a stoichiometric amount of 2,2,6,6-tetramethylpiperidinylmagnesium chloride·lithium chloride (TMPMgCl·LiCl) (1.0 M) at 0 °C. The Mg/H exchange reaction was performed at 0 °C for 30 min. A Ni(dppe)Cl_2 solution was then added to the reaction mixture, which was prepared just before use by mixing $Ni(PPh_3)_2Cl_2$ and 1,3-bis(diphenylphosphino)ethane to dehydrated THF (4−5 mL) in a 20 mL round-bottom flask purged with N_2. The mixture was allowed to stand at room temperature−60 °C for 2−6 h to undergo polymerization. After quenching the polymerization with 5 M aq HCl (1 mL), the solution was poured into methanol/water (300:100 mL) in a 500 mL beaker to precipitate the polymer. After filtration, the collected polymer was purified via Soxhlet extraction with methanol, acetone, and hexane and recovered with chloroform. The chloroform solution was passed through a short silica gel column to remove residual metal contaminants and condensed using a rotary evaporator followed by freeze-drying from its absolute benzene solution to afford the purified polymer.

P3EHTT (27k). Polymerization: at 60 °C for 6 h. Purple-colored powder. Yield: 0.177 g, 54%. M_n (target) = 30,000, M_n (SEC) = 26,500, $Đ_M$ = 1.40. R.R. = 99%. ^{1}H NMR (600 MHz, $C_2D_2Cl_4$, δ, ppm): 7.43 (s, Th-4*H* (H-T)), 2.97 (m, $-SCH_2-$), 1.65 (m, $-SCH_2CH-$), 1.58−1.10 (m, other $-CH_2-$), 0.95 (m, $-CH_3$).

P3HT (26k). Polymerization: at 40 °C for 2 h. Purple-colored powder. Yield: 0.174 g, 75%. M_n (target) = 25,000, M_n (SEC) = 26,200, $Đ_M$ = 1.20. R.R. = 99%. ^{1}H NMR (400 MHz, $CDCl_3$, δ, ppm): 6.98 (s, Th-4*H* (H-T)), 2.79 (m, Th-CH_2-), 1.69 (m, $ThCH_2CH_2-$), 1.50−1.20 (m, other $-CH_2-$), 0.90 (m, $-CH_3$).

P3DT (26k). Polymerization: at room temperature for 2 h. Purple-colored powder. Yield: 0.164 g, 55%. M_n (target) = 25,000, M_n (SEC) = 26,000, $Đ_M$ = 1.10. R.R. = 99%. ^{1}H NMR (400 MHz, $CDCl_3$, δ, ppm): 6.98 (s, Th-4*H* (H-T)), 2.79 (m, Th-CH_2-), 1.69 (m, $ThCH_2CH_2-$), 1.50−1.20 (m, other $-CH_2-$), 0.86 (m, $-CH_3$).

P3EHT (23k). Polymerization: at room temperature for 3 h. Red-colored powder. Yield: 0.176 g, 50%. M_n (target) = 25,000, M_n (SEC) = 22,800, $Đ_M$ = 1.20. R.R. = 99%. ^{1}H NMR (400 MHz, $CDCl_3$, δ, ppm): 6.92 (s, Th-4*H* (H-T)), 2.71 (m, Th-CH_2-), 1.69 (m, $ThCH_2CH-$), 1.40−1.10 (m, other $-CH_2-$), 0.88 (m, $-CH_3$).

OFET Fabrication and Characterization. The OFETs with solution-sheared films of **P3ATT**s and **P3AT**s were fabricated to evaluate the intrinsic *p*-type mobility, and the method for semiconducting polymer thin-film processing was similar to that reported previously.[19,51] Highly doped Si substrates with thermally grown 300-nm-thick SiO_2 were sonicated successively in acetone, 2-propanol, and deionized water and then passivated using a 0.1% solution of octadecyltrichlorosilane (ODTS) in toluene at room temperature for 90 min. The polymer semiconductor solution was dissolved in a mixed solvent of chlorobenzene/chloroform (3:97 v/v) at a concentration of 10 mg mL^{-1} heated at 55 °C for 30 min and deposited via the solution-shearing method with a fast shearing speed of 1−3 mm s^{-1} and a deposition temperature of 25 °C followed by annealing at 55 °C overnight under vacuum to remove the bulk solvent from the sample. Finally, a 60-nm-thick gold electrode was deposited via evaporation through a shadow mask at a base pressure of $<10^{-6}$ Torr. The final device architecture from bottom to top for these bottom-gate top-contact (BGTC) OFETs was Si/OTDS-treated SiO_2/polymer semiconductor/Au. All the OFET character-

https://doi.org/10.1021/acsami.1c04404
ACS Appl. Mater. Interfaces 2021, 13, 31898−31909

Scheme 1. Synthetic Routes for (a) P3HTT and P3DTT and (b) P3EHTT, P3HT, P3DT, and P3EHT.

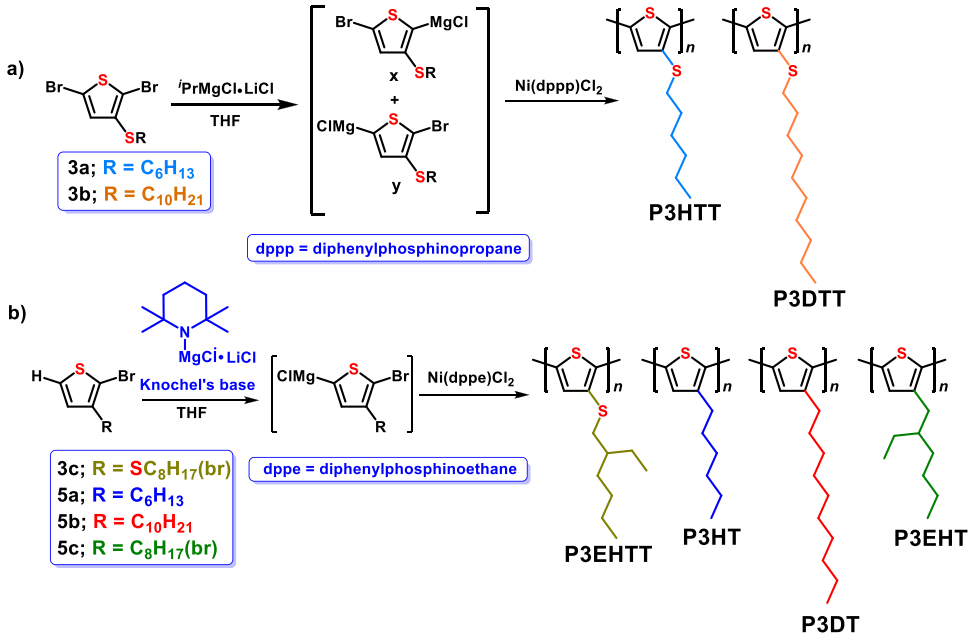

istics were measured using a Keithley 4200 semiconductor parametric analyzer inside a nitrogen-purged glove box to guarantee reproducibility. The mobility (μ) of the OFET devices was obtained by fitting the following equation to the saturation region of the transfer characteristic curves: $I_d = (W/2\ L)\ C_i\ \mu\ (V_g - V_{th})^2$, where W is the channel width (1500 μm), L is the channel length (20 μm), C_i is the gate dielectric layer capacitance per unit area (11 nF cm^{-2}), V_g is the gate voltage, V_{th} is the threshold voltage, and I_d is the drain current.

RESULTS AND DISCUSSION

Three regioregular **P3ATT**s were synthesized by adopting GRIM polymerization and Ni-catalyzed polycondensation using Knochel's base from monomers such as **3a**–**3c** (see Supporting Information for the synthetic procedure) with different alkylthio chain lengths ($R = -SC_6H_{13}$, $-SC_{10}H_{21}$, and $-SC_8H_{17}$(br)) and denoted **P3HTT**, **P3DTT**, and **P3EHTT**, respectively, via the modification of a previously reported procedure.[48] The synthetic routes are depicted in Scheme 1a,b, and the polymerization results are summarized in Table 1. The R.R. values of the resulting **P3HTT** were calculated from the signal intensity ratio corresponding to the 4-*H* thiophene proton at 7.4–7.5 ppm (head-to-tail) and 7.1–7.3 ppm (others) in the 600 MHz ^{1}H NMR spectra measured in deuterated 1,1,2,2-tetorachloroethane-d_2 ($C_2D_2Cl_4$) at 100 °C, and found to be in the range of 68–84% depending on the polymerization temperature (see Figure 1a for the representative ^{1}H NMR spectrum of **P3HTT (15k)**, Figures S2–S6 for other samples, and Figure S7 for the SEC UV traces for all the **P3HTT** samples). The relatively low R.R. values are probably due to there being less chemoselectivity in the Mg-Br exchange reaction between 2,5-dibromo-(3-hexylthio)thiophene and isopropylmagnesium chloride·lithium chloride (^{i}PrMgCl·LiCl) in tetrahydrofuran (THF), where a 43–58% and 57–42% Mg-Br exchange occurs at the 2- and 5-positions, respectively.[34] It was found that the increase in polymerization temperature improves the M_n of the obtained **P3HTT**s, but with the concomitant lowering of R.R. and increasing $Đ_M$, which indicates low polymerization controllability. In particular, the obvious trade-off between the R.R. and M_n values (see Figure 2) implies that a higher R.R. prevents further propagation of the reaction at the end of GRIM polymerization, thus limiting the M_n of the resulting polymers. In fact, insoluble materials emerged in the polymerization apparatus in all cases at the end of polymerization, probably because of the high intermolecular interaction of **P3HTT**. Similar results and trade-offs could also be confirmed in the case of **P3DTT** by extending the linear side chains to decylthio groups (Scheme 1, Table 1, Figure 2, and Figures S8–S11). Nevertheless, we succeeded in obtaining soluble **P3HTT (15k)** and **P3DTT (18k)** samples with relatively high M_n and moderate R.R. > 76% for OFET fabrication.

To improve the solubility of **P3ATT**s, a typical 2-ethyhexyl branched side chain group was introduced into the new thiophene monomer, 2-dibromo-(3-(2-ethylhexyl)thio)-thiophene. Furthermore, Ni-catalyzed polycondensation was employed using Knochel's base for the completely regioselective H/MgCl exchange at the 5-position of the monomer.[36] Consequently, regioregular **P3EHTT** could be synthesized with a high R.R. of 99% while maintaining a high M_n of 26,500 and good solubility due to the branched side chain (Table 1 and Figure S12). While the use of Knochel's base in the synthesis of **P3HTT** and **P3DTT** facilitated the selective H/MgCl exchange reactions at the 5-position of the monomer, insoluble oligomeric materials were obtained via precipitation before the propagation reactions were completed, possibly because of the very high crystallinity of the resulting linear-side-chain-based polymers with high R.R. and therefore coplanar main chains. The ^{1}H NMR spectrum of **P3EHTT (27k)** is presented in Figure 1b, showing the sharp singlet signal at 7.43 ppm and doublet signals at 2.97 ppm assignable to one proton at the 4-position of the thiophene ring and two protons of the methylene protons next to the thioether unit, respectively, confirming the quite high regioregularity of **P3EHTT (27k)**. These samples break the trade-off between M_n and R.R. as mentioned above (Figure 2). Thus, both the polymerization method and the side chain architecture are important for the practical synthesis of high-molecular-weight regioregular **P3ATT**s. For comparison, high-molecular-weight

https://doi.org/10.1021/acsami.1c04404
ACS Appl. Mater. Interfaces 2021, 13, 31898–31909

Table 1. The Results of Grignard Exchange Reaction and Synthesis of P3HTT, P3DTT, and P3EHTT.

		polymerization[b]				
polymer	Mg/Br exchange[a] x:y (%)	temp[c] (°C)	M_n (target)[d]	M_n (SEC)[e]	$Đ_M$ (SEC)[e]	R.R. (%)[f]
P3HTT (8k)	43:57	rt	30,000	8300	1.33	84
P3HTT (10k)	45:55	60	10,000	10,400	1.40	74
P3HTT (13k)	53:47	40	30,000	13,200	1.47	78
P3HTT (14k)	52:48	60	15,000	14,000	1.47	77
P3HTT (15k)	52:48	60	50,000	15,000	1.50	76
P3HTT (20k)	58:42	100[g]	50,000	20,200	1.73	68
P3DTT (10k)	41:59	rt	20,000	10,100	1.25	86
P3DTT (12k)	48:52	60	15,000	12,400	1.25	77
P3DTT (18k)	55:45	60	20,000	17,700	1.29	78
P3EHTT (27k)[h]	0:100[i]	rt	30,000	26,500	1.40	99
P3HT (26k)[h]	0:100[i]	rt	25,000	26,200	1.20	99
P3DT (26k)[h]	0:100[i]	rt	25,000	26,000	1.10	99
P3EHT (23k)[h]	0:100[i]	rt	25,000	22,800	1.2100	99

[a]The Grignard exchange reactions of 2,5-dibromo-(3-hexylthio)-thiophene with an equivalent of ^{i}PrMgCl·LiCl were carried out in THF under a N_2 atmosphere. *x* and *y* indicate the ratio of 3-alkylthio-5-bromothiophene (Grignard exchange at the 2-position) and 3-alkylthio-2-bromothiophene (Grignard exchange at the 5-position) in the products after quenching with HCl aq as determined by ^{1}H NMR. [b]Carried out in THF under a N_2 atmosphere. [c]Polymerization temperature. [d]Calculated as follows: M_n (target) = molecular weight of monomer repeating unit × $[\text{monomer}]_0/[\text{Ni catalyst}]_0$. [e]Determined by SEC using a calibration with polystyrene standards. [f]Determined by ^{1}H NMR (600 MHz) in $C_2D_2Cl_4$ at 100 °C. [g]The polymerization was carried out in 1,4-dioxane. [h]The Ni-catalyzed polycondensation was employed using Knochel's base. [i]The regioselective dehydration at the 5-position of the monomer in the Mg/H exchange reaction.

regioregular **P3HT**, **P3DT**, and **P3EHT** polymers were synthesized from monomers such as **5a−5c** (see Supporting Information for the synthetic procedure) via a similar Ni-catalyzed polycondensation using Knochel's base, as depicted in Scheme 1b (see Figures S13−S15 for ^{1}H NMR spectra and Figure S16 for SEC traces). The high thermal stability of all the studied samples for device fabrication was confirmed by TGA, with 5 wt % loss temperature ($T_{d,5\%}$) values in the range of 317−345 °C for **P3ATT**s, although they are lower than those of **P3AT**s ($T_{d,5\%}$ = 427−445 °C), probably due to the existence of heteroatom-based thiophene-S-alkyl linkages in **P3ATT**s (Figure S17 and Table S1). There were no transition peaks in the DSC thermograms of the **P3ATT**s (Figure S18 and Table S1).

Three **P3ATT** polymers, **P3HTT (15k)**, **P3DTT (18k)**, and **P3EHTT (27k)**, were used for the described experiments to characterize the thin-film properties. The **P3AT** and **P3ATT** solutions resulted in a color change in the solution from bright orange to dark purple (Figure 3a), which is indicative of different types of polymer aggregation. The assembly behavior of the polythiophenes, depending on the side chains, was probed using UV−vis spectroscopy. Figure 3b,c presents the optical absorption spectra of the **P3ATT** and **P3AT** solutions and the corresponding films, respectively. The optical properties of the synthesized polymers are summarized in Table 2. The **P3AT**s dissolve well in the solutions to form isolated chains, resulting in a single low-absorption band at 440−450 nm. All **P3ATT** solutions exhibited broad absorption in the range of 400−650 nm, with two distinct high- and low-energy bands. The measured absorption maxima (λ_{max} (soln)) of **P3HTT**, **P3DTT**, and **P3EHTT** were 515, 516, and 559 nm, respectively, with a vibronic shoulder at 609, 617, and 610 nm, respectively, indicative of a strong intermolecular interaction between **P3ATT** backbones that can induce prominent molecular aggregation in the solution. The similarity of the absorption spectra for **P3HTT** and **P3DTT** shows that changing the length of the alkylthio group from hexyl to decyl has a weak effect on the optical properties of the polymer. Besides, the temperature-dependent absorption of **P3ATT** in the solution was also performed to investigate the aggregation behavior, as shown in Figure S19. All three **P3ATT**s yield the blue-shifted absorption band and decreased absorption and decreased absorption intensity when increasing the temperature from 20 to 70 °C. These achieve the aggregation behavior attributed to the strong noncovalent molecular interaction. In addition, the fact that there were almost no longer changes in the absorption spectra when the temperature reaches 70 °C indicates the disaggregation in the single molecular **P3ATT** state. The absorption of **P3EHTT** at 70 °C was red-shifted by ∼16 nm when compared with **P3HTT** and **P3DTT**, implying that its backbone is more coplanar. The UV−vis spectra of all solution-sheared thin films show similar red-shifted absorption spectra and more noticeable vibronic shoulders at higher wavelengths, which reveal structural ordering in the solid state (Figure 3c). All the **P3ATT** thin films with alkylthio side chains feature red-shifted structured absorption and a more distinctive low energy 0−0 transition with respect to the alkylated-**P3AT**s. The absorption spectra of the **P3HTT** and **P3DTT** thin films show distinct absorption maxima (λ_{max} (film)) at 568 and 571 nm and a shoulder at 618 and 621 nm, which are assigned to the 0−1 and 0−0 vibronic transitions, respectively. The similarity of the solid-state absorption spectra also suggests that increasing the length of the alkylthio group from hexyl to decyl has a weak effect on the molecular aggregation. However, the branched side chain derivative **P3EHTT** has a maximum at 614 nm, accompanied by a less intense 0−1 peak at 561 nm, indicating that the absorption caused by the interchain transition is dominated by the intrachain (backbone) transition. The formation of vibrational fine structures in the **P3ATT**s was mainly due to the enhanced molecular S···S and S···π interactions, which increased the extent of coupling between and across the π-conjugated chromophore segments, giving rise to intermolecular packing and related structured absorption. A similar trend was noted for the bandgap determined from the absorption onset, with values from 1.87 to 2.18 eV, thus further suggesting that alkylthio side chain manipulation strongly impacts the aggregation tendency of the polymers. Owing to the high regioregularity and strong intermolecular interaction, the interchain electronic coupling between **P3EHTT** chains cannot be disrupted even though bulky branched alkylthio side chains are attached. In contrast,

https://doi.org/10.1021/acsami.1c04404
ACS Appl. Mater. Interfaces 2021, 13, 31898−31909

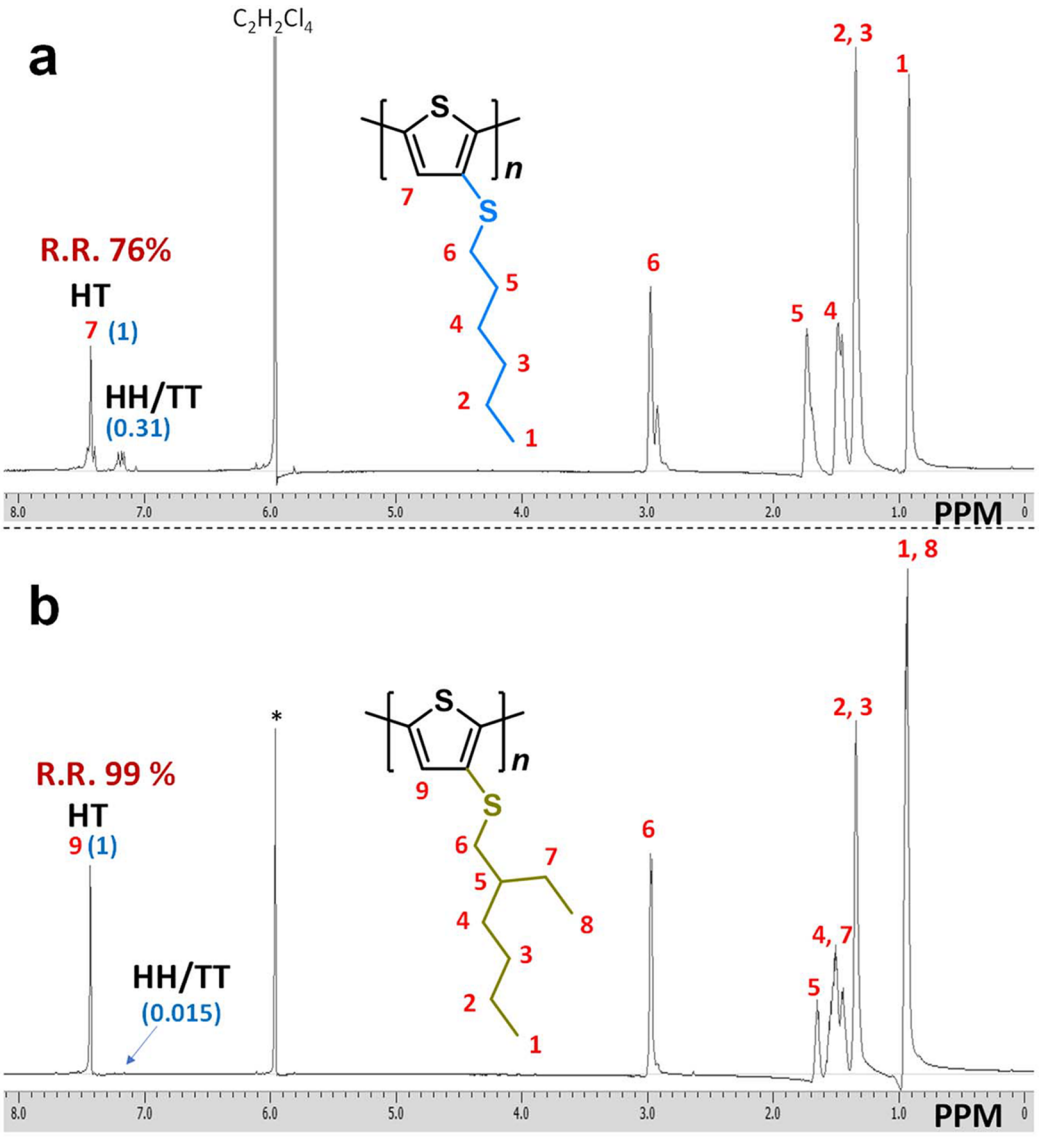

Figure 1. ^{1}H NMR spectra of (a) **P3HTT** (**15k**) and (b) **P3EHTT** (**27k**).

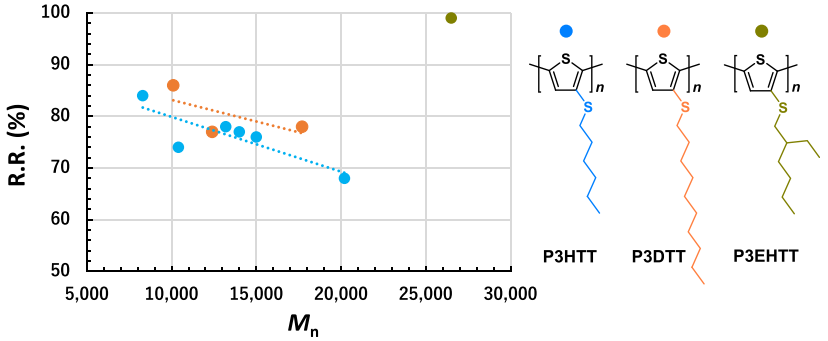

Figure 2. Plots of R.R. vs M_n of **P3HTT**, **P3DTT**, and **P3EHTT**.

P3EHT showed the most blue-shifted absorption peaks, mainly due to the presence of steric distortion in the conjugated backbones hindered by the branched alkyl side chain.[52] Thus, the most apparent difference in the λ_{max} for **P3EHTT** and the corresponding **P3EHT** can be observed in the absorption spectra of polythiophenes with branched side chains. Here, we can conclude that the incorporation of alkylthio side chains enhances molecular interactions and strengthens the tendency to aggregate between the conjugated backbones.

The molecular ordering and conjugation length along the polythiophene chains were quantitatively analyzed by intensity ratio of the 0−0 and 0−1 transitional peaks (A_{0-0}/A_{0-1}). We see that the A_{0-0}/A_{0-1} values of the **P3ATT** films are

https://doi.org/10.1021/acsami.1c04404
ACS Appl. Mater. Interfaces 2021, 13, 31898−31909

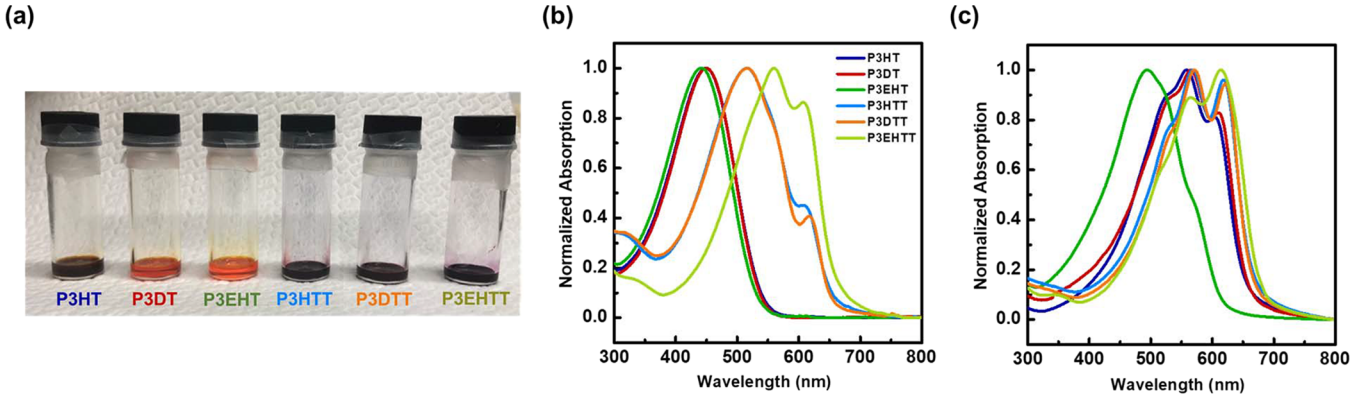

Figure 3. (a) Photograph of **P3AT** and **P3ATT** solutions. Normalized UV−vis absorption spectra of **P3ATT**s and **P3AT**s in (b) diluted cosolvent solutions and (c) thin films.

Table 2. The Optical Properties and HOMO/LUMO Energies of P3ATTs and P3ATs.

polymer	λ_{max} (soln) (nm)	λ_{max} (film) (nm)	A_{0-0}/A_{0-1}	E_g (eV)	E_{HOMO} (eV)	E_{LUMO} (eV)
P3HT	449	558	0.81	1.94	−4.74	−2.80
P3DT	450	565	0.83	1.93	−4.79	−2.86
P3EHT	441	494	0.50	2.18	−5.10	−2.92
P3HTT	515	568	0.96	1.90	−4.94	−3.04
P3DTT	516	571	0.94	1.90	−4.98	−3.08
P3EHTT	559	614	1.12	1.87	−4.90	−3.03

consistently lower than those of **P3AT**, suggesting an increase in the effective conjugation length and degree of interchain coupling within aggregates.[53] Especially for the case of **P3EHTT**, the A_{0-0}/A_{0-1} value of 1.1 (larger than unity) indicates an appreciable change in the conjugation length and long-range interchain interaction between the **P3EHTT** that are closely packed.[54] These results suggest that when incorporating the alkylthio side chain, a significant red-shifted absorption is observed along with an increase in A_{0-0}/A_{0-1}, which promotes increased and favorable intermolecular interactions.

The HOMO of all **P3ATT**s and **P3AT**s was measured via photoelectron spectroscopy in air (PESA; Figure S20), and the data are summarized in Table 2. By combining the data from PESA with the optical bandgap of the UV−vis spectrum, the LUMO was estimated. All the energy levels are provided in Figure S21. The HOMO energies of **P3ATT**s move downward with respect to those of **P3AT**s, which agree well with previously reported trends.[21,50]

The surface morphology of the polymer thin films was monitored via POM and AFM. Uniform solution-sheared morphologies can be found in the optical microscope images. The POM images were taken when the films were rotated 0 and 45° to the analyzing polarizer, as shown in Figure 4. It is evident from Figure S22 that there is no change in color and contrast in the POM images of the **P3DT**, **P3EHT**, **P3HTT**, and **P3DTT** films for any rotation angle. However, bright birefringence textures under cross polarizers were observed when both the **P3HT** and **P3EHTT** films were rotated to the crossed polarization axes. This change in optical brightness between crossed polarizers indicates that the resultant films were highly oriented.[55] The high regioregularity (more extended chains) of **P3HT** and **P3EHTT** allows the chains to be well aligned under shearing, and the resultant orientation

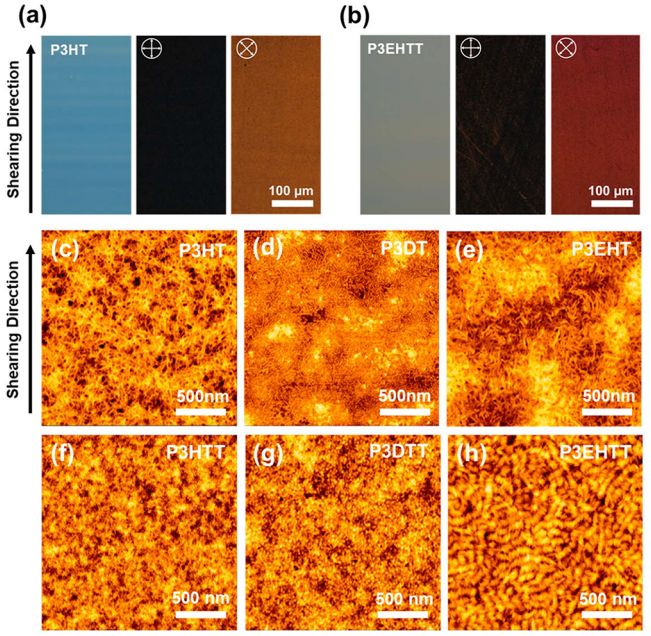

Figure 4. OM (left) and POM images of the (a) **P3HT** and (b) **P3EHTT** with solution-shearing direction at 0° (central) and 45° (right) with respect to the polarized analyzer. Tapping-mode AFM images of solution-sheared (c) **P3HT**, (d) **P3DT**, (e) **P3EHT**, (f) **P3HTT**, (g) **P3DTT**, and (h) **P3EHTT** films.

can be maintained during the solvent evaporation process due to their high molecular weights (longer chain relaxation times).[56] AFM height images of the **P3ATT** and **P3AT** solution-sheared thin films are shown in Figure 4 to examine the nanoscale morphologies. The observation of a randomly entangled nanofibrillar network in the **P3HT**, **P3DT**, and **P3EHT** films implies the existence of polymer crystallites.[57] In addition, it is evident that nanofibrils are distributed in-plane due to the $\pi-\pi$ stacking of polymer chains during the shearing process. Notably, all the AFM images of the **P3ATT** films revealed more densely packed nanofibrils, demonstrating enhanced aggregation through the introduction of alkylthio side chains. In particular, shear coating of the **P3EHTT** film results in macroscopic nanofibrils, which is also consistent with the results observed in the POM and absorption spectra. In addition, the increased surface roughness of **P3HT** and **P3EHTT** (2.51 and 2.06 nm, respectively) as compared with deposited films from other samples (0.73−1.50 nm) may be

https://doi.org/10.1021/acsami.1c04404
ACS Appl. Mater. Interfaces 2021, 13, 31898−31909

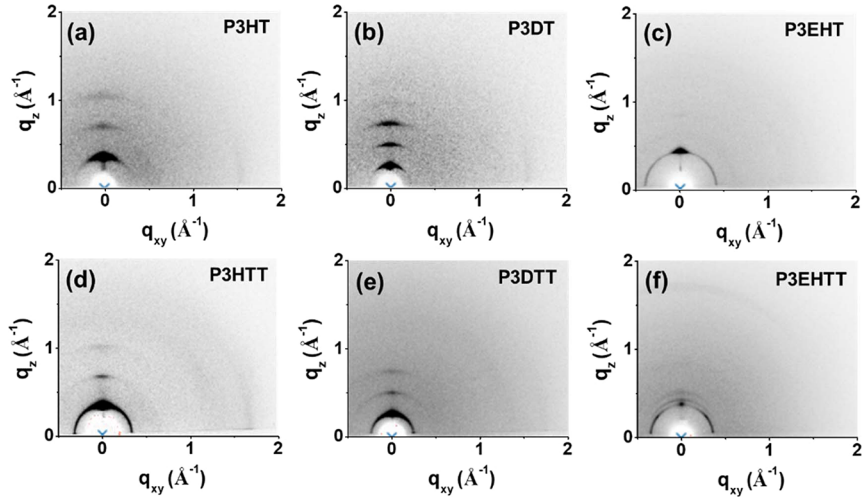

Figure 5. Two-dimensional GIXRD patterns of (a) **P3HT**, (b) **P3DT**, (c) **P3EHT**, (d) **P3HTT**, (e) **P3DTT**, and (f) **P3EHTT** recorded for the incident X-ray oriented parallel to the shearing direction.

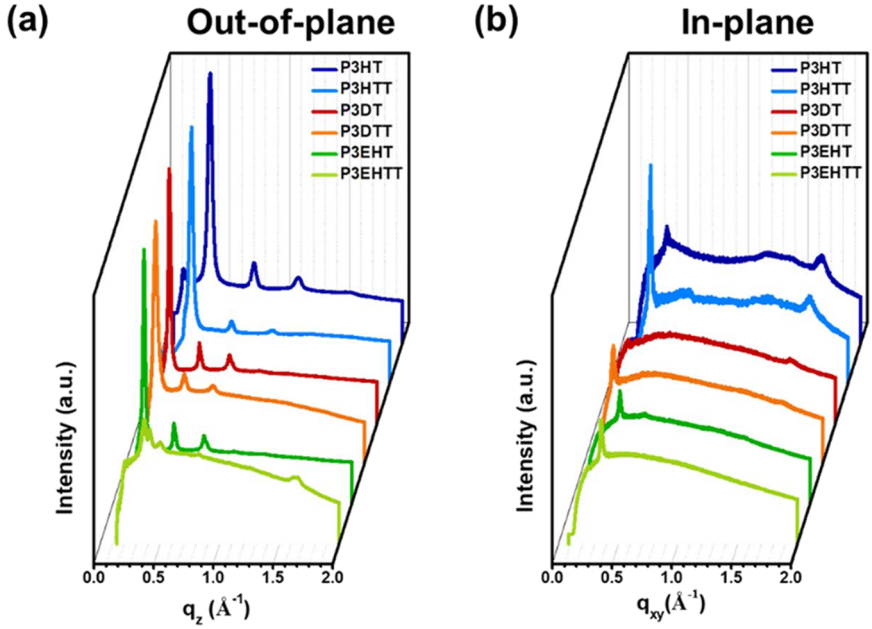

Figure 6. (a) Out-of-plane (q_z) and (b) in-plane (q_{xy}) one-dimensional scattering profile derived from two-dimensional scattering images of solution-sheared **P3TT** and **P3ATT** thin films.

Table 3. Crystallographic Parameters and OFET Performance of P3ATs and P3ATTs.

	crystallographic parameters		OFET parameters			
polymer	d_{100} (Å)	d_{010} (Å)	μ_{max} (cm^2 V^{-1} s^{-1})	μ_{avg} (cm^2 V^{-1} s^{-1})	I_{ON}/I_{OFF} (−)	V_{th} (V)
P3HT	16.97	3.88	2.14×10^{-1}	$(1.69 \pm 0.19) \times 10^{-1}$	10^5–10^6	5.45 ± 8.11
P3DT	24.15	3.88	7.41×10^{-2}	$(6.66 \pm 0.51) \times 10^{-2}$	10^4–10^5	1.03 ± 4.52
P3EHT	15.31	/	3.05×10^{-4}	$(2.40 \pm 0.74) \times 10^{-4}$	10^2–10^3	8.80 ± 8.22
P3HTT	18.51	3.76	1.48×10^{-2}	$(1.01 \pm 0.18) \times 10^{-2}$	10^3–10^4	-26.4 ± 4.05
P3DTT	25.14	3.78	7.68×10^{-3}	$(5.89 \pm 0.96) \times 10^{-3}$	10^3–10^4	-19.4 ± 18.4
P3EHTT	17.05	3.77	1.47×10^{-3}	$(7.98 \pm 3.41) \times 10^{-4}$	10^3–10^4	-3.84 ± 12.4

attributed to the increased quantity of nanofibril aggregates caused by the increased crystallinity.[58,59]

Grazing incidence X-ray diffraction (GIXRD) analysis was performed on the solution-sheared films to provide insight into the detailed microstructure and crystallinity of the thin films. Figure 5 and Figure S24b show the two-dimensional GIXRD patterns of **P3ATs** and **P3ATTs** with the incident X-rays parallel and perpendicular to the shearing direction, respectively. The one-dimensional lineouts taken along the out-of-plane (q_z) and in-plane (q_{xy}) scattering directions are also shown in Figure 6 and Figure S24c. Table 3 summarizes the resulting lamellar spacing (d_{100}) and π–π stacking

https://doi.org/10.1021/acsami.1c04404
ACS Appl. Mater. Interfaces 2021, 13, 31898−31909

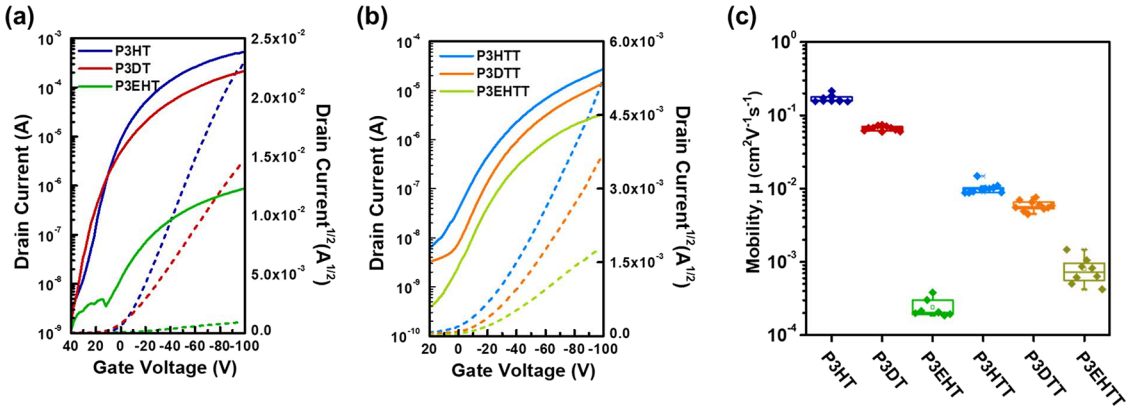

Figure 7. Transfer plot of (a) **P3AT** and (b) **P3ATT** OFET devices. (c) Comparison of mobility for all **P3AT** and **P3ATT** OFETs.

distances (d_{010}) of all synthesized polymers. The two-dimensional GIXRD images in Figure 5a,b,d,e exhibit a dominant edge-on backbone texture in the **P3HT**, **P3DT**, **P3HTT**, and **P3DTT** films with multiple Bragg diffraction peaks up to (300) along the out-of-plane direction as well as pronounced (010) $\pi-\pi$ stacking along the in-plane direction. Figure S24a depicts the possible chain alignment in the edge-on lamellar orientation for the four samples. The (010) diffraction peak corresponding to the periodicity of the $\pi-\pi$ stacking can be observed only when the angle between the incident X-ray and shearing direction is parallel (defined as 0°; Figure S24c), whereas this peak is quite weak when the X-ray is perpendicular to the shearing direction (defined as 90°; Figure S24c). These results confirm that the π-conjugated polymer main chains of the film are uniaxially aligned along the shearing direction (Figure S24b), where the side chain stacking direction is normal to the substrate with the π-stack oriented in the substrate plane. It is qualitatively apparent that the increase in alkyl(thio) spacer in the side chain from hexyl (hexylthio) to decyl (decylthio) explains the increase in the interdigitated alkyl(thio) lamellar distance. Moreover, the increased lamellar *d*-spacings (d_{100}) in all **P3ATT**s with respect to **P3AT**s also indicate longer side chain stacking due to the introduction of the sulfur atom in the alkylthio side chain. A broad $\pi-\pi$ stacking peak is observed in-plane at the peak center positions of q = 1.62, 1.62, 1.67, and 1.66 Å^{-1} for **P3HT**, **P3DT**, **P3HTT**, and **P3DTT**, respectively, which correspond to $\pi-\pi$ stacking distances of 3.88, 3.88, 3.76, and 3.78 Å. The slightly shorter $\pi-\pi$ stacking distances (by ∼0.1 Å) in **P3HTT** and **P3DTT** also suggest that they are able to pack more efficiently than **P3HT** and **P3DT**. This is also confirmed by an increase in aggregate content due to the strong red shift of the absorption band with the alkylthio substitution on the side chain. For the branched side chain, both **P3EHT** and **P3EHTT** show relatively weak lamellar ordering of the side chain stacking. This indicates that the **P3EHTT** chains in the thin film prefer a face-on orientation, possibly due to the more coplanar backbones and the irregular side chain configuration. Particularly, **P3EHTT** shows an out-of-plane (010) peak at around 1.67 Å^{-1}, corresponding to a $\pi-\pi$ stacking distance of 3.77 Å, while **P3EHT** has no trace of this peak in both q_{xy} and q_z directions. The reduced $\pi-\pi$ distance with the introduction of the alkylthio side chain may potentially shorten the pathway for carrier migration in **P3EHTT** molecules as compared with the random orientation associated with the amorphous microstructure of **P3EHT** (as indicated by the less discernible crystalline peak intensities).

To correlate the aforementioned thin-film morphologies with the charge transport properties of solution-sheared **P3ATT** and **P3AT** thin films, BGTC OFETs were fabricated with standard dimensions and measured inside a nitrogen atmosphere. The output and transfer plots of the *p*-type **P3ATT** and **P3AT** OFETs are depicted in Figure 7 and Figure S23, and the calculated OFET figures of merit, including the field-effect mobility (μ), threshold voltage (V_{th}), and ON/OFF ratio (I_{ON}/I_{OFF}), are shown in Figure 7c and Table 3. The **P3HT**- and **P3DT**-based OFETs are expected to exhibit moderately high maximum mobilities (μ_{max}) of 2.14 × 10^{-1} and 7.41 × 10^{-2} cm^2 V^{-1} s^{-1}, respectively, with average mobilities (μ_{avg}) of (1.69 ± 0.19) × 10^{-1} and (6.66 ± 0.51) × 10^{-2} cm^2 V^{-1} s^{-1}, respectively. However, the **P3EHT**-based OFETs exhibited electrical mobilities degraded by 2−3 orders of magnitude, which are clearly due to the disruption of conjugation introduced by the branched alkyl side chain in the twisted thiophene backbone.[58,59] The mobility in alkylthio-substituted **P3ATT** OFETs follows trends similar to those exhibited by **P3AT** OFETs in the following order: **P3HTT** > **P3DTT** > **P3EHTT**. Thus, $\mu_{max}(\mu_{avg})$ falls from 1.48 × 10^{-2} ((1.01 ± 0.18) × 10^{-1}) cm^2 V^{-1} s^{-1} for **P3HTT** to 7.68 × 10^{-3} ((5.89 ± 0.96) × 10^{-3}) cm^2 V^{-1} s^{-1} for **P3DTT** and 1.47 × 10^{-3} ((7.98 ± 3.41) × 10^{-3}) cm^2 V^{-1} s^{-1} for **P3DTT**. Both the mobilities of **P3HT** and **P3HTT** with smaller alkyl side chain lengths (−C_6H_{13} or −SC_6H_{13}) were enhanced compared to those of the **P3DT** and **P3DTT** counterparts with longer side chains (−C_8H_{17} or −SC_8H_{17}). Thus, the longer insulating linear side chains of **P3DT** and **P3DTT** may not be beneficial for charge transport, although they have a packing motif similar to that of **P3HT** and **P3HTT**.[60] A comparison of the **P3ATT** and **P3AT** series reveals that the mobility in **P3HTT** and **P3DTT** still lags behind that in **P3HT** and **P3DT**, even though strong molecular interactions can be observed based on absorption spectra and AFM morphologies, and a decreased $\pi-\pi$ stacking distance can be obtained. The main reason for the mobility reduction of the **P3HTT** and **P3DTT** samples is the regiorandomness due to their limited solubility, which decreases the crystallinity and π-conjugated backbone alignment. Although the mobility of the **P3HTT** OFETs is not as high as expected, it should be noted that regiorandom **P3HT** with a similar regioregularity of ∼77% showed a peak charge mobility of ∼10^{-4} cm^2 V^{-1} s^{-1},[61] which is 100 times lower than that of the **P3HTT** OFETs studied here. With the aid of a

https://doi.org/10.1021/acsami.1c04404
ACS Appl. Mater. Interfaces 2021, 13, 31898−31909

branched side chain to overcome the solubility issue, the comparable high regioregularity of **P3EHTT** and **P3EHT** results in the former having a 3 times higher mobility than the latter. It can be seen that the introduction of an alkylthio side chain helps in the formation of S···S and S···π interactions and enhances the charge transport properties in the polythiophene films. The I_{ON}/I_{OFF} increases in the range of 10^2 to 10^6, depending on the electric field-induced ON state I_d of the devices. The large negative V_{th} of the **P3HTT** and **P3DTT** OFETs probably arises from the presence of defects caused by the regiorandomness. This study provides a guideline for the molecular design of side chain engineering, and alkylthio-substituted polythiophene has a positive effect on device performance.

CONCLUSIONS

In summary, we have shown that noncovalent S···S and S···π molecular interactions are caused by the functionalization of the alkylthio side chain in semiconducting regioregular polythiophenes. The effects of additional sulfur atoms attached to alkyl chains of different lengths and branching on the aggregation behavior, molecular packing, nanoscale morphologies, and their solid-state electronic behaviors were systematically investigated. A series of **P3AT**s and **P3ATT**s were synthesized by considering the lengths of the alkyl/alklythio spacer consisting of **P3HT**/**P3DT** and **P3HTT**/**P3DTT** and bulky branched moieties consisting of **P3EHT** and **P3EHTT**. Comparison of the **P3ATT**s with the **P3AT** variants demonstrates that the alkylthio-substituted side chain has a pronounced effect on the aggregation/self-assembly behavior and frontier energy levels. The corresponding charge transport properties can also be connected to the thin-film morphologies and crystalline microstructures investigated by POM/AFM images and GIXRD, respectively. The use of **P3HT** and **P3HTT** results in a significantly increased charge mobility in OFET devices compared to **P3DT** and **P3DTT** with the longer side chain spacer and **P3EHT** and **P3EHTT** with branched side chains. The enhanced aggregation and decreased π–π stacking distance in **P3HTT** and **P3DTT** do not lead to any increase in the thin-film crystalline order and mobility compared to alkylated **P3HT** and **P3DT**, mainly because of their regiorandomness. Only the obtained regioregular **P3EHTT** has a higher mobility than the low-crystallinity **P3EHT** counterpart, as **P3EHTT** exhibits the face-on stacking mode. Our study highlights that the incorporation of noncovalent S···S and S···π interactions to control the conformation of regioregular polythiophenes is a useful way to optimize the solid-state structural organization and effective charge carrier transport in a range of electronic devices.

ASSOCIATED CONTENT

Supporting Information

The Supporting Information is available free of charge at https://pubs.acs.org/doi/10.1021/acsami.1c04404.

Materials and measurements, synthesis of monomers and polymers, ^{1}H NMR charts, SEC traces, TGA/DSC thermograms, molecular frontier orbital energies, PESA measurements, OM/POM images, output plot, and GIXRD patterns (PDF)

AUTHOR INFORMATION

Corresponding Authors

Ming-Chou Chen − *Department of Chemistry and Research Center of New Generation Light Driven Photovoltaic Modules, National Central University, Taoyuan 32001, Taiwan;* orcid.org/0000-0001-9033-0131; Email: mcchen@ncu.edu.tw

Cheng-Liang Liu − *Department of Materials Science and Engineering, National Taiwan University, Taipei 10617, Taiwan;* orcid.org/0000-0002-8778-5386; Email: liucl@ntu.edu.tw

Tomoya Higashihara − *Department of Organic Materials Science, Graduate School of Organic Materials Science, Yamagata University, Yonezawa, Yamagata 992-8510, Japan;* orcid.org/0000-0003-2115-1281; Email: thigashihara@yz.yamagata-u.ac.jp

Authors

Po-Shen Lin − *Department of Materials Science and Engineering, National Taiwan University, Taipei 10617, Taiwan*

Yamato Shoji − *Department of Organic Materials Science, Graduate School of Organic Materials Science, Yamagata University, Yonezawa, Yamagata 992-8510, Japan*

Shakil N. Afraj − *Department of Chemistry and Research Center of New Generation Light Driven Photovoltaic Modules, National Central University, Taoyuan 32001, Taiwan*

Mitsuru Ueda − *Department of Organic Materials Science, Graduate School of Organic Materials Science, Yamagata University, Yonezawa, Yamagata 992-8510, Japan*

Ching-Hsuan Lin − *Department of Chemistry and Research Center of New Generation Light Driven Photovoltaic Modules, National Central University, Taoyuan 32001, Taiwan*

Shin Inagaki − *Department of Organic Materials Science, Graduate School of Organic Materials Science, Yamagata University, Yonezawa, Yamagata 992-8510, Japan*

Taiki Endo − *Department of Organic Materials Science, Graduate School of Organic Materials Science, Yamagata University, Yonezawa, Yamagata 992-8510, Japan*

Shih-Huang Tung − *Institute of Polymer Science and Engineering, National Taiwan University, Taipei 10617, Taiwan;* orcid.org/0000-0002-6787-4955

Complete contact information is available at: https://pubs.acs.org/10.1021/acsami.1c04404

Author Contributions

$^{\perp}$P.-S.L., Y.S., and S.N.A. contributed equally to this work.

Notes

The authors declare no competing financial interest.

ACKNOWLEDGMENTS

M.-C.C. thanks the funding provided by MOST (109-3111-8-008-001) and the NCU-DSM Research Center. C.-L.L. gratefully acknowledges the funding from the Young Scholar Fellowship Program (Columbus Program) by the Ministry of Science and Technology (MOST) in Taiwan under Grant MOST 110-2636-E-002-021. T.H. thanks the Japan Society for the Promotion of Science (JSPS: KAKENHI 19 K22211) and Tokuyama Science Foundation for the financial support. The authors thank Beamline B13A1/B17A1/B23A1 from the

National Synchrotron Radiation Research Center (NSRRC) of Taiwan for providing beam time. This article was subsidized for English editing by National Taiwan University under the Excellence Improvement Program for Doctoral Students (Grant 108-2926-I-002-002-MY4) sponsored by the Ministry of Science and Technology, Taiwan.

REFERENCES

(1) Tsumura, A.; Koezuka, H.; Ando, T. Macromolecular Electronic Device: Field-effect Transistor with A Polythiophene Thin Film. *Appl. Phys. Lett.* **1986**, *49*, 1210−1212.
(2) Sirringhaus, H. 25th Anniversary Article: Organic Field-effect Transistors: The Path beyond Amorphous Silicon. *Adv. Mater.* **2014**, *26*, 1319−1335.
(3) Wang, C.; Dong, H.; Hu, W.; Liu, Y.; Zhu, D. Semiconducting π-Conjugated Systems in Field-effect Transistors: A Material Odyssey of Organic Electronics. *Chem. Rev.* **2012**, *112*, 2208−2267.
(4) Ashizawa, M.; Zheng, Y.; Tran, H.; Bao, Z. Intrinsically Stretchable Conjugated Polymer Semiconductors in Field Effect Transistors. *Prog. Polym. Sci.* **2020**, *100*, 101181.
(5) Sariciftci, N. S.; Smilowitz, L.; Heeger, A. J.; Wudl, F. Photoinduced Electron Transfer from A Conducting Polymer to Buckminster-fullerene. *Science* **1992**, *258*, 1474−1476.
(6) Li, Z.'a.; Chueh, C.-C.; Jen, A. K.-Y. Recent Advances in Molecular Design of Functional Conjugated Polymers for High-performance Polymer Solar Cells. *Prog. Polym. Sci.* **2019**, *99*, 101175.
(7) Chen, J.; Chen, Y.; Feng, L.-W.; Gu, C.; Li, G.; Su, N.; Wang, G.; Swick, S. M.; Huang, W.; Guo, X.; Facchetti, A.; Marks, T. J. Hole (Donor) and Electron (Acceptor) Transporting Organic Semiconductors for Bulk-heterojunction Solar Cells. *EnergyChem* **2020**, *2*, 100042.
(8) Zhao, W.; Ding, J.; Zou, Y.; Di, C.-A.; Zhu, D. Chemical Doping of Organic Semiconductors for Thermoelectric Applications. *Chem. Soc. Rev.* **2020**, *49*, 7210−7228.
(9) Fan, Z.; Ouyang, J. Thermoelectric Properties of PEDOT:PSS. *Adv. Electron. Mater.* **2019**, *5*, 1800769.
(10) Russ, B.; Glaudell, A.; Urban, J. J.; Chabinyc, M. L.; Segalman, R. A. Organic Thermoelectric Materials for Energy Harvesting and Temperature Control. *Nat. Rev. Mater.* **2016**, *1*, 16050.
(11) Kim, M.; Ryu, S. U.; Park, S. A.; Choi, K.; Kim, T.; Chung, D.; Park, T. Donor-acceptor-conjugated Polymer for High-performance Organic Field-effect Transistors: A progress Report. *Adv. Funct. Mater.* **2020**, *30*, 1904545.
(12) Yang, Y.; Liu, Z.; Zhang, G.; Zhang, X.; Zhang, D. The Effects of Side Chains on The Charge Mobilities and Functionalities of Semiconducting Conjugated Polymers Beyond Solubilities. *Adv. Mater.* **2019**, *31*, 1903104.
(13) Sun, H.; Guo, X.; Facchetti, A. High-performance n-Type Polymer Semiconductors: Applications, Recent Development, and Challenges. *Chem* **2020**, *6*, 1310−1326.
(14) Huang, H.; Yang, L.; Facchetti, A.; Marks, T. J. Organic and Polymeric Semiconductors Enhanced by Noncovalent Conformational Locks. *Chem. Rev.* **2017**, *117*, 10291−10318.
(15) Wadsworth, A.; Chen, H.; Thorley, K. J.; Cendra, C.; Nikolka, M.; Bristow, H.; Moser, M.; Salleo, A.; Anthopoulos, T. D.; Sirringhaus, H.; McCulloch, I. Modification of Indacenodithiophene-based Polymers and Its Impact on Charge Carrier Mobility in Organic Thin-film Transistors. *J. Am. Chem. Soc.* **2020**, *142*, 652−664.
(16) Vegiraju, S.; Torimtubun, A. A. A.; Lin, P.-S.; Tsai, H.-C.; Lien, W.-C.; Chen, C.-S.; He, G.-Y.; Lin, C.-Y.; Zheng, D.; Huang, Y.-F.; Wu, Y.-C.; Yau, S.-L.; Lee, G.-H.; Tung, S.-H.; Wang, C.-L.; Liu, C.-L.; Chen, M.-C.; Facchetti, A. Solution-processable Quinoidal Dithioalkylterthiophene-based Small Molecules Pseudo-pentathienoacenes via An Intramolecular S···S Lock for High-performance n-Type Organic Field-effect Transistors. *ACS Appl. Mater. Interfaces* **2020**, *12*, 25081−25091.
(17) Vegiraju, S.; Luo, X.-L.; Li, L.-H.; Afraj, S. N.; Lee, C.; Zheng, D.; Hsieh, H.-C.; Lin, C.-C.; Hong, S.-H.; Tsai, H.-C.; Lee, G.-H.; Tung, S.-H.; Liu, C.-L.; Chen, M.-C.; Facchetti, A. Solution Processable Pseudo n-Thienoacenes via Intramolecular S···S Lock for High Performance Organic Field Effect Transistors. *Chem. Mater.* **2020**, *32*, 1422−1429.
(18) Lin, C.-C.; Afraj, S. N.; Velusamy, A.; Yu, P.-C.; Cho, C.-H.; Chen, J.; Li, Y.-H.; Lee, G.-H.; Tung, S.-H.; Liu, C.-L.; Chen, M.-C.; Facchetti, A. A Solution Processable Dithioalkyl Dithienothiophene (DSDTT) Based Small Molecule and Its Blends for High Performance Organic Field Effect Transistors. *ACS Nano* **2021**, *15*, 727−738.
(19) Vegiraju, S.; Chang, B.-C.; Priyanka, P.; Huang, D.-Y.; Wu, K.-Y.; Li, L.-H.; Chang, W.-C.; Lai, Y.-Y.; Hong, S.-H.; Yu, B.-C.; Wang, C.-L.; Chang, W.-J.; Liu, C.-L.; Chen, M.-C.; Facchetti, A. Intramolecular Locked Dithioalkylbithiophene-based Semiconductors for High-performance Organic Field-effect Transistors. *Adv. Mater.* **2017**, *29*, 1702414.
(20) Salatelli, E.; Marinelli, M.; Lanzi, M.; Zanelli, A.; Dell'Elce, S.; Liscio, A.; Gazzano, M.; Maria, F. D. Bulk Heterojunction Solar Cells: The Role of Alkyl Side Chain on Nanoscale Morphology of Sulfur Over-rich Regioregular Polythiophene/Fullerene Blends. *J. Phys. Chem. C* **2018**, *122*, 4156−4164.
(21) Kozycz, L. M.; Gao, D.; Seferos, D. S. Compositional Influence on The Regioregularity and Device Parameters of A Conjugated Statistical Copolymer. *Macromolecules* **2013**, *46*, 613−621.
(22) Maria, F. D.; Gazzano, M.; Zanelli, A.; Gigli, G.; Loiudice, A.; Rizzo, A.; Biasiucci, M.; Salatelli, E.; D'Angelo, P.; Barbarell, G. Synthesis and Photovoltaic Properties of Regioregular Head-to-head Substituted Thiophene Hexadecamers. *Macromolecules* **2012**, *45*, 8284−8291.
(23) Barbarella, G.; Di Maria, F. Supramolecular Oligothiophene Microfibers Spontaneously Assembled on Surfaces or Coassembled with Proteins Inside Live Cells. *Acc. Chem. Res.* **2015**, *48*, 2230−2241.
(24) Pozo-Gonzalo, C.; Khan, T.; McDouall, J. J. W.; Skabara, P. J.; Roberts, D. M.; Light, M. E.; Coles, S. J.; Hursthouse, M. B.; Neugebauer, H.; Cravino, A.; Sariciftci, N. S. Synthesis and Electropolymerisation of 3′,4′-Bis(alkylsulfanyl)terthiophenes and The Significance of The Fused Dithiin Ring in 2,5-Dithienyl-3,4-ethylenedithiothiophene (DT-EDTT). *J. Mater. Chem.* **2002**, *12*, 500−510.
(25) Jeeva, S.; Lukoyanova, O.; Karas, A.; Dadvand, A.; Rosei, F.; Perepichka, D. F. Highly Emissive and Electrochemically Stable Thienylene Vinylene Oligomers and Copolymers: An Unusual Effect of Alkylsulfanyl Substituents. *Adv. Funct. Mater.* **2010**, *20*, 1661−1669.
(26) Li, Y.; Zhong, Y.; Jiang, H.; Rath, T.; Wang, Q.; Ehmannd, H. M. A.; Trimmel, G.; Wen, S.; Zhang, Y.; Yang, R. The Effect of Alkylthio Substituents on The Photovoltaic Properties of Conjugated Polymers. *Org. Electron.* **2019**, *68*, 50−55.
(27) Maria, F. D.; Zangoli, M.; Gazzano, M.; Fabiano, E.; Gentili, D.; Zanelli, A.; Fermi, A.; Bergamini, G.; Bonifazi, D.; Perinot, A.; Caironi, M.; Mazzaro, R.; Morandi, V.; Gigli, G.; Liscio, A.; Barbarella, G. Controlling The Functional Properties of Oligothiophene Crystalline Nano/Microfibers via Tailoring of The Self-assembling Molecular Precursors. *Adv. Funct. Mater.* **2018**, *28*, 1801946.
(28) Motherwell, W. B.; Moreno, R. B.; Pavlakos, I.; Arendorf, J. R. T.; Arif, T.; Tizzard, G. J.; Coles, S. J.; Aliev, A. E. Noncovalent Interactions of π Systems with Sulfur: The Atomic Chameleon of Molecular Recognition. *Angew. Chem., Int. Ed.* **2018**, *57*, 1193−1198.
(29) Glass, R. S.; Adamowicz, L.; Broeker, J. L. Theoretical Studies on Transannular sulfur.cntdot..cntdot..cntdot.sulfur Interactions in Geometrically Constrained 1,5-Dithiocane Derivatives. *J. Am. Chem. Soc.* **1991**, *113*, 1065−1072.
(30) Beno, B. R.; Yeung, K.-S.; Bartberger, M. D.; Pennington, L. D.; Meanwell, N. A. A Survey of The Role of Noncovalent Sulfur Interactions in Drug Design. *J. Med. Chem.* **2015**, *58*, 4383−4438.
(31) Wang, X.-Y.; Jiang, W.; Chen, T.; Yan, H.-J.; Wang, Z.-H.; Wana, L.-J.; Wang, D. Molecular Evidence for The Intermolecular S···

https://doi.org/10.1021/acsami.1c04404
ACS Appl. Mater. Interfaces 2021, 13, 31898−31909

S Interaction in The Surface Molecular Packing Motifs of A Fused Thiophene Derivative. *Chem. Commun.* **2013**, *49*, 1829−1831.
(32) Tsuzuki, S.; Orita, H.; Sato, N. Intermolecular Interactions of Oligothienoacenes: Do S···S Interactions Positively Contribute to Crystal Structures of Sulfur-containing Aromatic Molecules? *J. Chem. Phys.* **2016**, *145*, 174503.
(33) Flores-Huerta, A. G.; Tkatchenko, A.; Galván, M. Nature of Hydrogen Bonds and S···S Interactions in The L-cystine Crystal. *J. Phys. Chem. A* **2016**, *120*, 4223−4230.
(34) McCullough, R. D.; Lowe, R. D. Enhanced Electrical Conductivity in Regioselectively Synthesized Poly(3-alkylthiophenes). *J. Chem. Soc., Chem. Commun.* **1992**, 70−72.
(35) McCullough, R. D.; Lowe, R. D.; Jayaraman, M.; Anderson, D. L. Design, Synthesis, and Control of Conducting Polymer Architectures: Structurally Homogeneous Poly(3-alkylthiophenes). *J. Org. Chem.* **1993**, *58*, 904−912.
(36) Chen, T. A.; Rieke, R. D. The First Regioregular Head-to-tail Poly(3-hexylthiophene-2,5-diyl) and A Regiorandom Isopolymer: Nickel versus Palladium Catalysis of 2(5)-Bromo-5(2)-(bromozincio)-3-hexylthiophene Polymerization. *J. Am. Chem. Soc.* **1992**, *114*, 10087−10088.
(37) Chen, T.-A.; Wu, X.; Rieke, R. D. Regiocontrolled Synthesis of Poly(3-alkylthiophenes) Mediated by Rieke Zinc: Their Characterization and Solid-state Properties. *J. Am. Chem. Soc.* **1995**, *117*, 233−244.
(38) Persson, N. E.; Chu, P.-H.; McBride, M.; Grover, M.; Reichmanis, E. Nucleation, Growth, and Alignment of Poly(3-hexylthiophene) Nanofibers for High-performance OFETs. *Acc. Chem. Res.* **2017**, *50*, 932−942.
(39) Yokoyama, A.; Miyakoshi, R.; Yokozawa, T. Chain-growth Polymerization for Poly(3-hexylthiophene) with A Defined Molecular Weight and A Low Polydispersity. *Macromolecules* **2004**, *37*, 1169−1171.
(40) Miyakoshi, R.; Yokoyama, A.; Yokozawa, T. Catalyst-transfer Polycondensation. Mechanism of Ni-catalyzed Chain-growth Polymerization Leading to Well-defined Poly(3-hexylthiophene). *J. Am. Chem. Soc.* **2005**, *127*, 17542−17547.
(41) Sheina, E. E.; Liu, J.; Iovu, M. C.; Laird, D. W.; McCullough, R. D. Chain Growth Mechanism for Regioregular Nickel-initiated Cross-coupling Polymerizations. *Macromolecules* **2004**, *37*, 3526−3528.
(42) Iovu, M. C.; Sheina, E. E.; Gil, R. R.; McCullough, R. D. Experimental Evidence for The Quasi-"living" Nature of The Grignard Metathesis Method for The Synthesis of Regioregular Poly(3-alkylthiophenes). *Macromolecules* **2005**, *38*, 8649−8656.
(43) Chang, J.-F.; Sun, B.; Breiby, D. W.; Nielsen, M. M.; Sölling, T. I.; Giles, M.; McCulloch, I.; Sirringhaus, H. Enhanced Mobility of Poly(3-hexylthiophene) Transistors by Spin-coating from High-boiling-point Solvents. *Chem. Mater.* **2004**, *16*, 4772−4776.
(44) Li, G.; Shrotriya, V.; Huang, J.; Yao, Y.; Moriarty, T.; Emery, K.; Yang, Y. High-efficiency Solution Processable Polymer Photovoltaic Cells by Self-organization of Polymer Blends. *Nat. Mater.* **2005**, *4*, 864−868.
(45) Wu, X.; Chen, T.-A.; Rieke, R. D. A study of small band gap polymers: Head-to-tail Regioregular Poly[3-(alkylthio)thiophenes] Prepared by Regioselective Synthesis Using Active Zinc. *Macromolecules* **1996**, *29*, 7671−7677.
(46) Vandeleene, S.; Van den Bergh, K.; Verbiest, T.; Koeckelberghs, G. Influence of The Polymerization Methodology on The Regioregularity and Chiroptical Properties of Poly(alkylthiothiophene)s. *Macromolecules* **2008**, *41*, 5123−5131.
(47) Krasovskiy, A.; Krasovskaya, V.; Knochel, P. Mixed Mg/Li Amides of The Type $R_2NMgCl{\cdot}LiCl$ as Highly Efficient Bases for The Regioselective Generation of Functionalized Aryl and Heteroaryl Magnesium Compounds. *Angew. Chem., Int. Ed.* **2006**, *45*, 2958−2961.
(48) Wang, P.; Jeon, I.; Lin, Z.; Peeks, M. D.; Savagatrup, S.; Kooi, S. E.; Voorhis, T. V.; Swager, T. M. Insights into Magneto-optics of Helical Conjugated Polymers. *J. Am. Chem. Soc.* **2018**, *140*, 6501−6508.
(49) Maria, F. D.; Olivelli, P.; Gazzano, M.; Zanelli, A.; Biasiucci, M.; Gigli, G.; Gentili, D.; Angelo, P. D.; Cavallini, M.; Barbarella, G. A Successful Chemical Strategy to Induce Oligothiophene Self-assembly into Fibers with Tunable Shape and Function. *J. Am. Chem. Soc.* **2011**, *133*, 8654−8661.
(50) Huo, L.; Zhou, Y.; Li, Y. Alkylthio-substituted Polythiophene: Absorption and Photovoltaic Properties. *Macromol. Rapid Commun.* **2009**, *30*, 925−931.
(51) Vegiraju, S.; Lin, C.-Y.; Priyanka, P.; Huang, D.-Y.; Luo, X.-L.; Tsai, H.-C.; Hong, S.-H.; Yeh, C.-J.; Lien, W.-C.; Wang, C.-L.; Tung, S.-H.; Liu, C.-L.; Chen, M.-C.; Facchetti, A. Solution-processed High-performance Tetrathienothiophene-based Small Molecular Blends for Ambipolar Charge Transport. *Adv. Funct. Mater.* **2018**, *28*, 1801025.
(52) Boudouris, B. W.; Ho, V.; Jimison, L. H.; Toney, M. F.; Salleo, A.; Segalman, R. A. Real-time Observation of Poly(3-alkylthiophene) Crystallization and Correlation with Transient Optoelectronic Properties. *Macromolecules* **2011**, *44*, 6653−6658.
(53) Clark, J.; Chang, J.-F.; Spano, F. C.; Friend, R. H.; Silva, C. Determining Exciton Bandwidth and Film Microstructure in Polythiophene Films Using Linear Absorption Spectroscopy. *Appl. Phys. Lett.* **2009**, *94*, 163306.
(54) Rahimi, K.; Botiz, I.; Agumba, J. O.; Motamen, S.; Stingelin, N.; Reiter, G. Light Absorption of Poly(3-hexylthiophene) Single Crystals. *RSC Adv.* **2014**, *4*, 11121−11123.
(55) Molina-Lopez, F.; Wu, H.-C.; Nathan, G.-J.; Hongping, W.; Shaw, Y. L.; Xu, J.; Toney, M. F.; Bao, Z. Enhancing Molecular Alignment and Charge Transport of Solution-sheared Semiconducting Polymer Films by The Electrical-blade Effect. *Adv. Electron. Mater.* **2018**, *4*, 1800110.
(56) Qu, G.; Zhao, X.; Newbloom, G. M.; Zhang, F.; Mohammadi, E.; Strzalka, J. W.; Pozzo, L. D.; Mei, J.; Diao, Y. Understanding Interfacial Alignment in Solution Coated Conjugated Polymer Thin Films. *ACS Appl. Mater. Interfaces* **2017**, *9*, 27863−27874.
(57) Choi, D.; Chang, M.; Reichmanis, E. Controlled Assembly of Poly(3-hexylthiophene): Managing The Disorder to Order Transition on The Nano-through Mesoscales. *Adv. Funct. Mater.* **2015**, *25*, 920−927.
(58) Park, Y. D.; Lee, H. S.; Choi, Y. J.; Kwak, D.; Cho, J. H.; Lee, S.; Cho, K. Solubility-induced Ordered Polythiophene Precursors for High-performance Organic Thin-film Transistors. *Adv. Funct. Mater.* **2009**, *19*, 1200−1206.
(59) Zhao, K.; Khan, H. U.; Li, R.; Su, Y.; Amassian, A. Entanglement of Conjugated Polymer Chains Influences Molecular Self-assembly and Carrier Transport. *Adv. Funct. Mater.* **2013**, *23*, 6024−6035.
(60) Babel, A.; Jenekhe, S. A. Alkyl Chain Length Dependence of The Field-effect Carrier Mobility in Regioregular Poly(3-alkylthiophene)s. *Synth. Met.* **2005**, *148*, 169−173.
(61) Sirringhaus, H.; Brown, P. J.; Friend, R. H.; Nielsen, M. M.; Bechgaard, K.; Langeveld-Voss, B. M. W.; Spiering, A. J. H.; Janssen, R. A. J.; Meijer, E. W.; Herwig, P.; de Leeuw, D. M. Two-dimensional Charge Transport in Self-organized, High-mobility Conjugated Polymers. *Nature* **1999**, *401*, 685−688.

https://doi.org/10.1021/acsami.1c04404
ACS Appl. Mater. Interfaces 2021, 13, 31898−31909